Soft Matter

PAPER

View Article Online
View Journal

Cite this: DOI: 10.1039/d5sm00597c

Effects of additives on the rheology and phase behavior of lamellar-structured concentrated surfactant solutions

Parth U. Kelkar, [a] Matthew Kaboolian, [a] Cornelius A. Atherton, [a] Evan R. Williams, [a] Seth Lindberg [b] and Kendra A. Erk *[a]

Structure–property–processing relationships for model lamellar structured 70 wt% SLE_nS solutions were developed with a combination of rheometry, cross-polarized optical microscopy, calorimetry, small angle X-ray scattering, and rheo-ultrasonic speckle velocimetry. Additives were utilized to maintain high surfactant activity, reduce bulk viscosity and simplify processing. While the bulk flow behavior of neat SLE_nS solutions was similar, the effect of some additives was sensitive to the degree of ethoxylation. Linear-chain alcohols (C_2–C_5) partitioned into inter-bilayer water layers, dehydrating surfactant headgroups and inducing lamellar-to-micellar transitions. Short-chain polyols formed higher-viscosity hexagonal and mixed phases at room temperature through hydrogen bonding with surfactant headgroups. Heating beyond the upper temperature limit weakened these interactions, resulting in low-viscosity solutions. Within the lamellar phase, common salt promoted shear-induced crystallization above the equilibrium temperature range. Propylene glycol suppressed shear-induced crystallization and promoted wall-slip under shear, forming lubrication layers near the wall. These strategies offer practical levers to tune rheology and microstructure of concentrated surfactant systems, with the datasets developed providing a foundation for future modeling. Outcomes from this study inform the sustainable design and efficient processing of concentrated surfactant-based products.

Received 10th June 2025,
Accepted 30th July 2025

DOI: 10.1039/d5sm00597c

rsc.li/soft-matter-journal

Introduction

Surfactants are the primary active ingredients in consumer and industrial cleaning products, such as shampoos, laundry detergents, dishwashing liquids and hard surface cleaners.[1,2] In recent years, there has been a growing push toward concentrated formulas – products designed with higher levels of active ingredients like surfactants and minimal water content. This marks a departure from traditional formulations, where water typically constituted most of the product volume.[3] Reducing or eliminating water from a product expands the design space, enabling the inclusion of actives that are otherwise unstable or insoluble in aqueous solutions.[4] The move toward higher activity formulas is also driven by well-established environmental and economic benefits: concentrates reduce water usage, packaging waste, lower transportation costs, and align with key sustainability goals.[5–7] A recent life cycle analysis of three dishwashing liquids found that the most concentrated detergent (~60% active) had the lowest environmental impact across several categories, as well as the lowest water consumption.[8]

Despite these benefits, concentrates introduce significant challenges that stem from the self-assembly of surfactant molecules.[9] As surfactant concentration increases, these systems undergo lyotropic transitions from low-viscosity, optically isotropic micellar phases to highly viscous, steady or shear birefringent liquid crystalline phases, such as hexagonal, cubic and lamellar structures.[10–12] Traditionally, the critical packing parameter (CPP) has provided a robust framework to model these transitions.[13] Although the more concentrated lamellar phase has a lower apparent steady shear viscosity (~10–20 Pa s at 20 °C, 1 s^{-1}) than the less concentrated hexagonal phase (~100 Pa s at 20 °C, 1 s^{-1}),[14,15] both exhibit yield and non-Newtonian flow behaviors and characteristic of highly ordered[16] liquid crystalline assemblies. These properties complicate a range of manufacturing operations starting from the unloading of raw feedstocks from delivery vehicles such as trucks and railcars. They also lead to difficulties in downstream processes like pumping, mixing, and bottling, as well as in meeting consumer-relevant performance criteria like dissolution in water.[17–19] A shear rate of 1 s^{-1} is frequently used as an

[a] School of Materials Engineering, Purdue University, West Lafayette, IN, 47907, USA. E-mail: erk@purdue.edu
[b] Corporate Engineering, The Procter & Gamble Company, West Chester, OH, 45069, USA

industrial benchmark, as it is above low-shear torque limits[20] and below the onset of inertial and turbulent effectss.[21,22] Numerically, viscosity below 1 Pa s at this shear rate is considered acceptable for reliable pouring and pumping. Formulating systems with high surfactant activity while maintaining low viscosity continues to be a central challenge in the development of next-generation consumer cleaning products.

Differences in rheological behavior across liquid crystalline phases have important implications for process design. Hexagonal phases, composed of cylindrical surfactant micelles packed into a hexagonal array are generally avoided due to poor responsiveness to applied shear forces and temperature.[15] Their inadvertent formation during manufacturing can cause pipe blockage, damage equipment, and lead to substantial economic losses.[23] In contrast, lamellar phases, comprising stacked surfactant bilayers separated by water layers, are used as high-activity feedstocks that can be more readily processed into concentrated surfactant-based products.[14,15,24–26]

The rheological behavior of lamellar systems, particularly highly concentrated lamellar-structured solutions, has been the focus of growing attention in recent years, with studies examining their response to temperature and applied shear across various surfactant chemistries. These trends have been reviewed by Berni *et al.*[27] and studied more recently by Kelkar *et al.*[28] Lamellar-structured anionic sodium lauryl ether sulfate (SLE_nS), where '*n*' denotes the degree of ethoxylation, at concentrations near 70 wt% surfactant in water has emerged as a model industrial feedstock due to its widespread use across product categories and commercial availability at scale. In contrast to sodium dodecyl sulfate (SDS),[29] it forms stable, highly concentrated lamellar phases at room temperature. However, while concentrated SLE_nS systems provide a versatile processing platform, their response to formulation-relevant additives remains poorly understood. This study investigates the effect of additives on the structure and rheology of concentrated lamellar SLE_nS solutions. To address persistent challenges, trajectories through complex phase spaces were developed to reduce viscosity and improve the processability of high-active model feedstocks used in consumer cleaning products.

Background

Sodium lauryl ether sulfate (SLE_nS) is a key surfactant across the personal cleansing and fabric care business, and recent studies have increasingly focused on its aqueous lamellar phase. Caicedo-Casso *et al.* mapped the concentration dependent (20–70 wt%) room temperature phase behavior of SLE_1S–water and identified a lamellar phase from 60–70 wt% surfactant. The flow behavior was characterized by shear rheometry and the presence of flow instabilities such as wall slip and plug flow were monitored with rheo-ultrasonic speckle velocimetry.[15] A similar study by Castaldo *et al.* investigated the effects of surfactant concentration on dissolution, phase behavior, and rheology. Although the degree of ethoxylation was not specified, the presence of a cubic (V_1) phase suggests that the system studied was SLE_3S–water.[30] Experimental phases reported by Caicedo-Casso *et al.* were further validated by Hendrikse *et al.* using dissipative particle dynamics and molecular dynamics.[31,32] Kelkar *et al.* explored the rheological and microstructural changes in neat 70 wt% SLE_1S solutions at low-temperatures and reported shear-induced crystallization effects on the complex viscosity. Ferraro *et al.* developed a temperature-concentration phase diagram (30–60 °C) of the SLE_3S–water system.[33,34] Their findings emphasized that molecular polydispersity within SLE_3S and SLE_1S, particularly in alkyl tail length, degrees of ethoxylation, sulfation and sulfonation, common in industrial-grade feedstocks,[35] could strongly influence phase and flow behavior.

Despite the growing body of work, most published studies remain focused on the bulk behavior of binary SLE_nS–water systems, whereas real-world products including simplified, essential-ingredient formulas are rarely that simple. Even the simplest commercial formulations contain additives that are used to modify viscosity, aid processing, or enhance stability and performance.[36] Along with traditionally recognized processing parameters (*e.g.*, equipment type, applied shear, pressure, and temperature ramps), the order and timing of additive incorporation can significantly affect material behavior. This represents another lever in the engineer's toolbox. For example, the 4-P+ process demonstrates how changing the order of addition, to post-adding polyols, polymers, preservatives, and perfumes as a premix in the aqueous phase can accelerate processing and improve stability.[37] While it may be desirable to understand the impact of every ingredient in a multicomponent formulation, this is rarely practical.

Adding a single ingredient to a surfactant–water feedstock transforms it into a ternary system. Unlike binary diagrams, ternary phase diagrams have historically been far more difficult to interpret, due in part to ambiguity in additive positioning and the tendency of systems near multiphase boundaries to undergo tie line hopping.[38] Despite these challenges, the breadth and depth of ternary phase science is remarkably rich. Foundational work by McBain and Elford[39] and Ekwall[40,41] on ionic surfactant–water–additive systems, laid the groundwork for understanding additive effects on phase behavior. Initial studies examined potassium oleate–water–potassium chloride systems, followed by sodium octanoate–water–decanol. For more detailed discussions of ternary phase diagrams across ionic, nonionic, and zwitterionic systems the reader is referred to reviews by Lisi and Milioto,[42] Laughlin *et al.*,[43] Khan,[44] Holmberg *et al.*,[45] Wennerström,[46] and Tucker.[47] While not intended to be exhaustive, significant historical investigations[48–61] and more recent studies by Akter *et al.*,[62] Baruah *et al.*,[63] Zhong *et al.*,[64] and Honaryar *et al.*,[65] into alcohol, electrolyte, cosurfactant and polymer induced transitions illustrate both the evolution and enduring complexity of ternary surfactant systems.

Within this broader body of work, a smaller subset of studies has explored the effects of additives on the structural and rheological behavior of lamellar phases. Work by Murthy and Kaler and Montalvo *et al.* extensively characterized the

cetyltrimethylammonium bromide (CTAB)–water system. The effects of alcohol tail length on the temperature dependent lamellar-to-isotropic phase transition,[66] and benzyl alcohol on the rheology were investigated.[67] Roux *et al.* worked with lamellar phases of the SDS–water–pentanol and dodecanol systems to study the role of membrane flexibility on undulation interactions between membranes.[52] The stability of lamellar phases as a function of inter- and intra-bilayer interactions in three anionic, cationic and non-ionic surfactant–water–propylene glycol systems were further investigated by Martino and Kaler.[68] Yang *et al.* used small-angle X-ray scattering to study the extent to which cyclohexane and benzene penetrated into the lamellar phase of the anionic surfactant dihydrogenated tallowalkyl dimethyl ammonium chloride (DHTDMAC).[69] Goncalves *et al.* focused on the effect of several additives on the lamellar gel phase (L_β) to more classical L_α phase transition for double-chain cationic surfactants dioctadecyldimethylammonium chloride (DODAC) and dioctadecyldimethylammonium bromide (DODAB).[70–72] Polymer–surfactant interactions in liquid crystals were reviewed by Piculell[73] and further experimentally investigated for SDS and CTAB–water–polyvinylpyrrolidone (PVP) by Cukurcent and Masalci.[74]

Despite its industrial relevance, the literature on ternary concentrated lamellar-structured SLE_nS systems is extremely limited. Khosharay *et al.*,[75] Choi *et al.*,[76] Pleines *et al.*,[77] Parker and Fieber[78] and Panoukidou *et al.*[79] reported additive driven changes in micellization, wormy micelle contour length and the salt curve in dilute solutions. Caicedo-Casso *et al.*[15] used common salt (NaCl) to form and characterize lamellar phases with 40 wt% SLE_1S while Kelkar *et al.* studied the effect of added NaCl on radial dissolution of feedstock lamellar pastes (70 wt% SLE_1S).[18]

The goal of this experimental study was to develop material relationships between industrially relevant additives (alcohols, acetates, short-chain aliphatic polyols, hydrotropes and desiccants) and concentrated (70 wt%) lamellar structured aqueous SLE_nS solutions. The bulk behavior of 70 wt% SLE_1S, SLE_2S, and SLE_3S was first characterized to establish structural and rheological baselines across degrees of ethoxylation and manufacturers. Three distinct processing strategies were developed to achieve high surfactant activity while reducing viscosity. In the first approach, short-chain linear alcohols induced lamellar-to-micellar transitions at room temperature. The second strategy used propylene glycol, glycerin, and 1,3-propanediol to drive lamellar-to-hexagonal or mixed-phase transitions, with elevated temperature enabling access to lower-viscosity zones. The third approach focused on processing within the lamellar regime, examining how propylene glycol and NaCl affected the microstructure, shear-induced crystallization, and the formation and evolution of flow instabilities like wall slip and plug flow.

Based on the initial baseline comparisons, SLE_3S was selected for the first two approaches, while SLE_1S was used for the third. Structural and rheological responses across all three strategies were characterized using a combination of shear and oscillatory rheometry, static and dynamic cross-polarized optical microscopy, small-angle X-ray scattering (SAXS), differential scanning calorimetry (DSC), and rheo-ultrasound speckle velocimetry (rheo-USV). Structure–property–processing relationships developed here provide a platform for rational formulation design, enabling control over phase behavior and rheology of concentrated surfactant systems.

Experimental section

Materials

Molecular structures of all surfactants and additives are presented in Fig. S1.

Surfactants

Lamellar-structured concentrated 70 wt% aqueous solutions of sodium lauryl ether sulfate (SLE_nS) –SLE_1S (STEOL® CS-170 UB), SLE_2S (STEOL® CS-270 Plus), and SLE_3S (STEOL® CS-370) were all obtained from the Stepan Company, and an industrial-grade 70 wt% SLE_3S paste (Kopacol® N70 LS ReNu Ultra) was supplied by the Procter & Gamble Company. All surfactants were used as received. The SLE_nS samples consisted of a homologous mixture of alkyl chains averaging 12 carbon atoms (ranging from C_{10} to C_{16}), with n corresponding to the average number of ethylene oxide (EO) units; for example, SLE_3S has an average of three ethoxy groups. Bulk rheological, thermal and phase characterization of feedstock SLE_1S, SLE_2S, and SLE_3S solutions (Fig. S2) revealed only minor differences in lamellar d-spacing due to EO chain length. SLE_1S (STEOL® CS-170 UB) and SLE_3S (Kopacol N70 LS ReNu Ultra) were used for all experiments with additives.

Additives

All additives were used without further purification. Short to medium-chain alcohols –ethanol (anhydrous, 200 proof, >99.5%), isopropyl alcohol (IPA) (≥ 99.0%), 1-butanol (99.8%), 1-pentanol (≥ 99%), and 1-hexanol (98%) were purchased from Sigma-Aldrich®, as were methyl acetate (≥ 99%), ethyl acetate (≥ 99.5%), propylene glycol (≥ 99.5%), 1,3-propanediol (98%), sodium chloride (NaCl) (≥ 99.0%), and sodium xylenesulfonate (SXS) (≥ 90%). Longer-chain alcohols, 1-octanol and 1-decanol (both 98%), were sourced from Alfa Aesar (now Thermo Scientific chemicals), while 1-dodecanol (98%) was obtained from Sigma-Aldrich Fine Chemicals (SAFC). Glycerin was supplied by the Procter & Gamble Company.

Sample preparation

The procedures described below are based on methodologies previously established by Caicedo-Casso *et al.*[15] and Kelkar *et al.*[18] All samples were prepared at room temperature in 20 g batches in glass vials by mixing the appropriate amount of additive with the lamellar paste. Liquid additives were incorporated at concentrations of 1%, 2.5%, 5%, 10%, 15%, and 20% by weight, while NaCl and SXS were added at 0.5%, 1%, 2%, 2.5%, 5%, and 10% by weight. All percentages were calculated based on the total mass of the surfactant and water

mixture. For all ternary mixtures, the SLE_nS : water ratio was held constant at 2.333, which resulted in final compositions (wt%) that varied with additive loading. For example, 2.5%, 10%, and 20% added additive yielded surfactant (S) : water (W) : additive (A) compositions of approximately 68.3(S) : 29.3(W) : 2.4(A), 63.6(S) : 27.3(W) : 9.1(A), and 58.3(S) : 25(W) : 16.7(A) respectively.

Equilibration times ranged from a minimum of 2 days to up to 7 days, with longer durations required for samples with NaCl or SXS. SLE_1S solutions were placed on a hot plate at approximately 35 °C, sealed with Parafilm® to minimize evaporation, and gently stirred at 24-hour intervals. Samples with SLE_3S were initially equilibrated in an industrial oven at the same temperature, also sealed with Parafilm® and subjected to the same stirring schedule. Sample homogeneity was assessed through direct visual inspection. Following equilibration, all SLE_3S + additive specimens were subjected to a thermal screening to assess susceptibility to temperature dependent phase transitions. Samples were kept at 45 °C for 48 h and then at 75 °C for an additional 48 h in a convection oven, with Parafilm® seal maintained throughout. A protorheological approach[80] was used to assess flow behavior *via* vial inversion and selected samples with lower apparent viscosities compared to the neat lamellar baseline were analyzed further.

Ultrasound speckle velocimetry (USV) measurements required seeding each sample with an ultrasonic contrast agent to enable velocity profile acquisition. The methodology was adapted from established protocols by Bice,[81] Caicedo-Casso *et al.*[15] and Manneville *et al.*[82] Hollow glass spheres (Sigma-Aldrich) with an average diameter of 11 μm and a density of 1.1 g·cm^{-3} were used. The total sample volume used for measurement was approximately 20 g and the concentration of these tracers was adjusted based on the sample type: micellar solutions (STEPANOL® WA-EXTRA – Stepan Company) used for calibration were seeded with 1 wt% glass spheres, while liquid crystalline (lamellar and hexagonal) specimens contained approximately 0.3 wt%. These concentrations were sufficiently low to assume that the particles followed the flow as Lagrangian tracers. Micellar samples were sonicated for approximately 10 minutes to ensure uniform dispersion of the tracer particles and were used immediately afterward. In contrast, liquid crystalline specimens were gently mixed by hand, degassed in a vacuum oven to eliminate entrained air bubbles, and likewise used immediately following preparation.

Methods

All experiments were conducted at Purdue University and the Corporate Engineering Technology Laboratories (CETL) of The Procter & Gamble Company. Sample transport between the two facilities was minimized to reduce handling variability. When necessary, most samples were first allowed to fully equilibrate at their site of preparation and subsequently rested for at least 24 hours upon arrival before being used in experiments.

Basic rheometry

Rheometry experiments used to measure bulk material behavior under steady and oscillatory flow, were performed using two instruments. At Purdue University, an Anton Paar MCR 702 Modular Compact Rheometer equipped with a CC10 concentric cylinder fixture (bob diameter = 10.0 mm, bob length = 14.9 mm, measurement gap = 0.422 mm) and Peltier temperature control was used. At Procter & Gamble, experiments were performed on a TA Instruments DHR-2 rheometer using a 40 mm, 2° cone-and-plate fixture with Peltier control. For temperature ramp comparisons, a DIN CC27.9 mm cup-and-bob fixture (bob diameter = 27.99 mm, measurement gap = 1.071 mm) was also used. No measurable evaporation effects were observed within the timescale of the experiments, and the cone geometry was selected to minimize sample volume. The specific fixture used for each dataset is noted in the corresponding figure.

All measurements were performed using fresh specimens from the same surfactant solution batch, conducted under steady-state conditions,[28] and repeated in triplicate; representative datasets are reported. Experimental protocols used in this study are similar to those previously used by Caicedo-Casso *et al.*[15] and Kelkar *et al.*[28] To ensure consistent shear history, samples were pre-sheared at 5 s^{-1} for 1 minute and rested for 2 minutes prior to testing. Rate controlled forward (0.1–100 s^{-1}) flow sweep experiments were performed (30 s per point, 10 points per decade, ±5% uncertainty on the DHR-2 and 7 s per point, 20 points per decade on MCR 702). The magnitude of applied oscillations during oscillatory measurements (strain amplitude, γ_0 = 0.1% and angular frequency, ω = 10 rad per s) was within the linear viscoelastic range (LVER) of the samples.[28] Unless specified otherwise, the temperature was changed at 1 °C min^{-1}, with an uncertainty of ±0.1 °C. To ensure reproducibility, rheometry experiments on selected samples were performed across multiple instruments and geometries. Rheological trends were consistent across cone-and-plate and concentric cylinder fixtures, as confirmed by flow curve and temperature ramp data (Fig. S3).

Advanced rheo-ultrasonic speckle velocimetry (rheo-USV)

USV is a one-dimensional velocity profiling technique that tracks the motion of contrast agents within a deforming specimen using high-frequency backscattered ultrasound. Measurements were performed at Purdue University using a custom-built USV system developed in collaboration with Sébastien Manneville,[82] coupled to an Anton Paar MCR 302 rheometer and a concentric cylinder cell (48 mm rotor, 0.83 mm gap) fabricated from polymethyl methacrylate. The cell and transducer were immersed in a temperature-controlled water bath to ensure uniform temperature and facilitate acoustic transmission. The USV system has a spatial resolution of ~42 μm, a temporal resolution ranging from 0.1 to 100 s and operates over a shear rate range of 0.2 to 200 s^{-1}. The physical configuration and full experimental procedure closely follow those reported previously by Caicedo-Casso *et al.*[15] and Bice.[81]

USV was conducted during shear-startup experiments. For each specimen, three decreasing shear rates were applied sequentially, each preceded by a corresponding pre-shear: 100 s^{-1} before 70 s^{-1}, 10 s^{-1} before 7 s^{-1}, and 1 s^{-1} before

0.7 s^{-1}. Pre-shear durations were at least 20 seconds, and velocimetry data were collected after a minimum of 30 seconds of shearing to ensure steady-state behavior. Geometrical calibration of the instrument and simple shear velocity profile of a Newtonian micellar solution is shown in Fig. S4. All experiments were conducted at 22 °C.

X-ray scattering

Small-angle X-ray scattering (SAXS) and wide-angle X-ray scattering (WAXS) measurements were conducted using an Anton Paar SAXSPOINT 2.0 system equipped with a Cu-α X-ray source and an Eiger detector. These techniques were used to probe nanoscale structural features: *d*-spacing and phase identification based on characteristic scattering patterns. High-viscosity liquid crystalline samples were loaded into the Anton Paar PasteCell N fixture with polycarbonate film windows and held inside a temperature-controlled TCStage 150. Low-viscosity samples were loaded into TCStage-compatible quartz cuvettes. Static phase characterization was carried out at 25 °C on key compositions including lamellar feedstocks with and without additives. Each measurement comprised three 2-minute exposures at sample-detector distances of 825 mm (SAXS) and 365 mm (WAXS).

For thermal phase change studies, samples were cooled from ambient to 20 °C at 1 °C min^{-1} and equilibrated for 2 minutes. They were then heated to target temperatures. Neat Kopacol SLE_3S was analyzed using the same protocol with sequential heating to match the range used for ternary systems of interest. At each temperature, samples were equilibrated for 2 minutes before exposure. The three-frame averaged two-dimensional scattering frames were reduced using Anton Paar's SAXSAnalysis software. One-dimensional, empty-cell-subtracted transmittance-normalized patterns were analyzed for characteristic peak structures, sizes, and positions.

Dynamic scanning calorimetry (DSC)

All experiments were performed using a TA Instruments Q2000 DSC and hermetically sealed Tzero aluminum pans and lids. DSC was used to measure heat flow during thermal phase transitions. Unless specified otherwise, the temperature was changed at a rate of 1 °C min^{-1}.

Static cross-polarized optical microscopy and shear-cell visualization

Static cross-polarized images were captured using a Keyence VHX-F series microscope equipped with a dual-objective VH-ZST Zoom Lens (magnification range 20× to 2000×) with polarizers. Qualitative phase identification was based on the work of Rosevear.[10] For *in situ* temperature ramping, a digitally controlled Linkam Peltier stage was mounted on the microscope. The initial and end temperatures, as well as the ramp speeds, were pre-programmed. Small volumes (~0.2 ml) of sample were carefully put on a glass slide, followed by 100 μm thick spacers and a cover slip.

Microstructural evolution with applied shear forces was captured using a CSS450 optical shearing system (Linkam Scientific, Tadworth UK). This is a parallel plate cell with quartz plates and a viewing window located at 7.5 mm off center; the gap and rotational velocity are electronically controlled with the Linksys32 software. The vertical gap was set to 75 μm. The stage was mounted on a Motic upright microscope (BA410E) with 5× LM Plan lens (NA 0.13) and 20× lens (NA 0.4). Images were acquired using a FLIR Blackfly 5 MP C-mount, color, USB camera through the FLIR Spinview software. Approximately 0.2 mL of sample was deposited at the center of the shear cell stage using a syringe, and the lid was carefully secured. The shear rate was increased stepwise from 0.1 s^{-1}, 1 s^{-1}, 10 s^{-1} with 5 s rest periods between each 30 s step. Images were collected every 250 milliseconds and stitched together.

Data analysis

Experimental data was fitted to theoretical models using Origin 2022 (OriginLab).

Results and discussion

Three processing strategies were developed to modify phase behavior and rheology in high-active surfactant pastes (Fig. 1): (1) lamellar-to-micellar transitions at room temperature, (2) lamellar-to-hexagonal or mixed-phase transition followed by heating to approach the upper temperature limit, and (3) effects of additives within the lamellar phase. In ternary surfactant–water–additive systems at constant temperature and pressure, the Gibbs phase rule limits coexistence to three phases.[83–85] Multiple two- and three-phase regions exist in a full diagram, and the law of alternates requires transitions between single-phase regions to pass through at least one two-phase region.[11] Fixing the surfactant-to-water ratio constrains the accessible phase space and excludes certain transitions[86] and isolates the effect of additives on the lamellar phase.

Approach 1: lamellar to micellar transitions

Short-chain linear alcohols were effective at disrupting the lamellar structure. With increasing ethanol (Fig. 2(a)) and IPA (Fig. 2(b)) concentration, the shear thinning behavior characteristic of the highly viscous lamellar phase transitioned to a high-shear rate low-viscosity Newtonian plateau at the highest added concentration.[15] Above 15 wt%, both ethanol and IPA induced a lamellar-to-micellar transition causing a decrease in viscosity. As seen in Fig. 3(f)–(h), birefringent, disordered lamellar phases were dispersed in an optically dark micellar background. These domains are readily homogenized even at low shear rates, resulting in a Newtonian plateau. This transition was also confirmed by SAXS (Fig. S5). As ethanol concentration increased, the lamellar *d*-spacing decreased from 44.6 ± 0.4 Å for neat 70 wt% SLE_3S to 40.3 ± 0.3 Å at 10 wt% ethanol, with a corresponding weakening of the lamellar structure. At 20 wt% ethanol, the system had a micellar separation distance of 37.4 ± 2.9 Å. At a fixed additive concentration (10 wt%), increasing alcohol chain length progressively increased the 1 s^{-1} viscosity – ~11 Pa s (ethanol), ~ 12 Pa s (IPA),

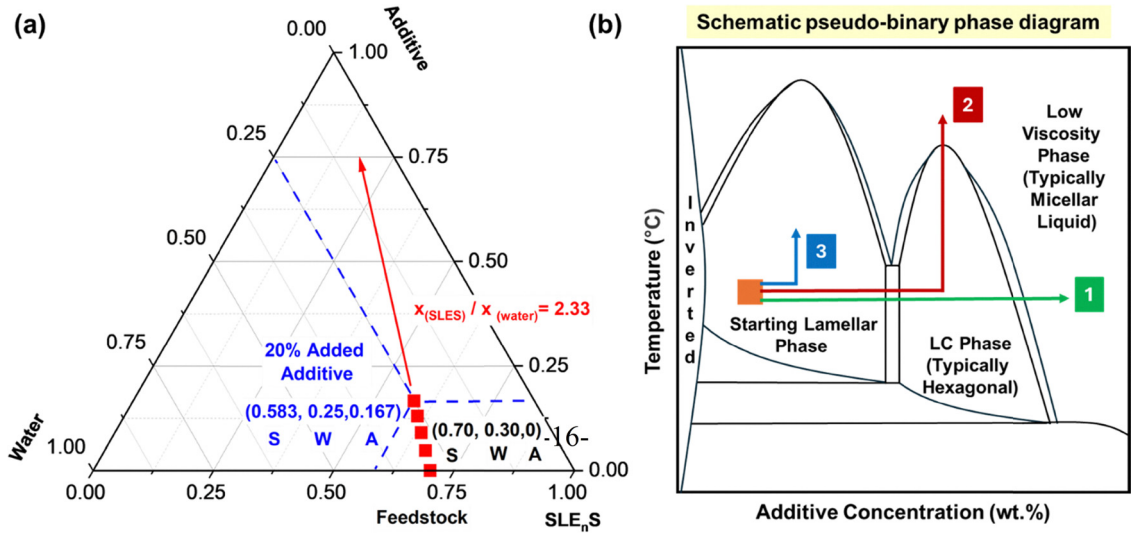

Fig. 1 (a) Ternary diagram showing feedstock lamellar concentration, constant surfactant/water ratio trajectories and effective surfactant (*S*) : water (*W*) : additive (*A*) composition with 20 wt% added additive, and (b) simplified, schematic pseudo-binary diagram illustrating the three experimental approaches used in this study. Adapted from Laughlin[11] and Yamashita.[87]

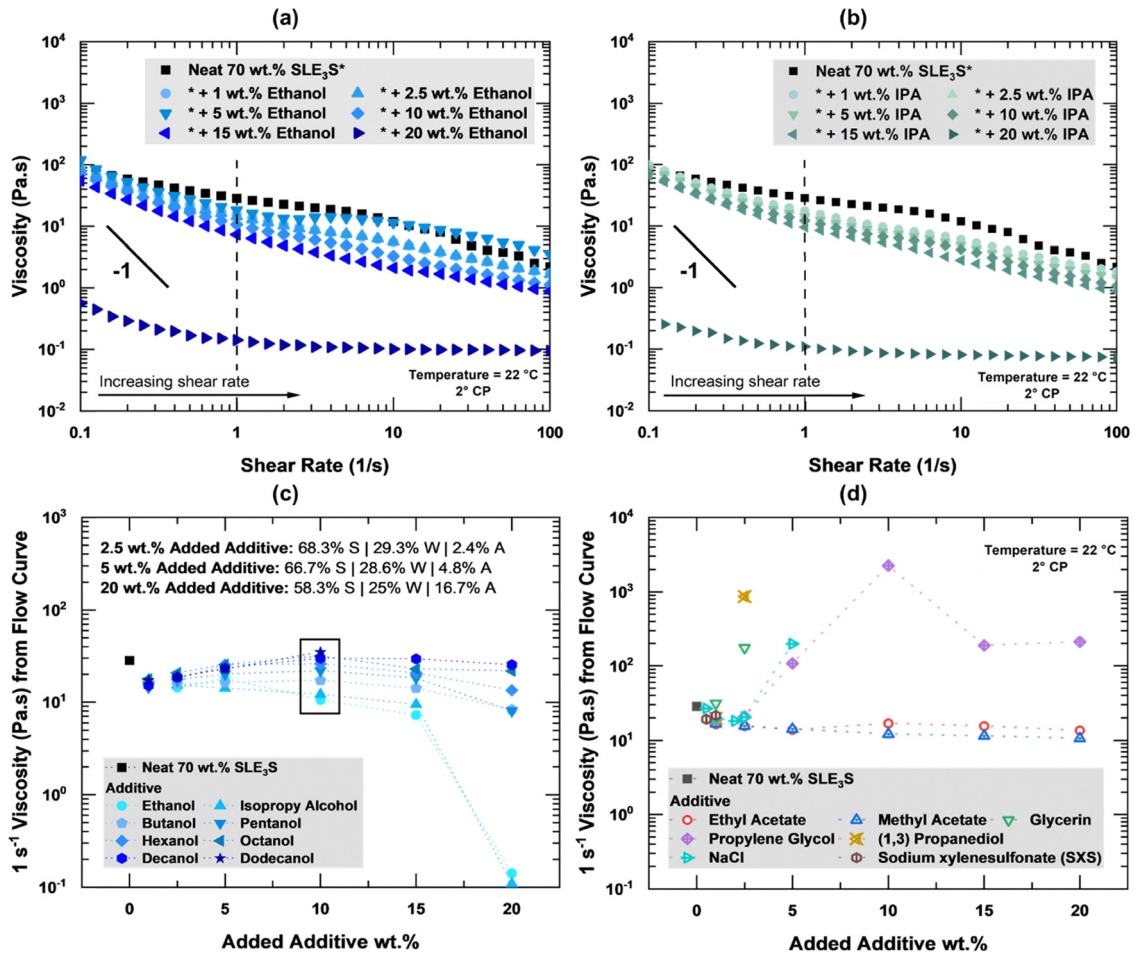

Fig. 2 Effect of added (a) ethanol and (b) isopropyl alcohol (IPA) on the rheology of feedstock lamellar pastes, (c) 1 s^{-1} viscosity with increasing linear alcohol chain length and (d) 1 s^{-1} viscosity with increasing concentrations of acetates, polyols, hydrotrope (SXS) and salt. Solid black lines represent a slope of −1. Measured viscosities have an uncertainty of ± 5% and all flow curves are presented in Fig. S6 and S7. Concentration and additive dependent phases, 1 s^{-1} viscosity, Herschel–Bulkley fits for shear stress *vs.* shear rate at low shear rates (Fig. S8) and *d*-spacings are all tabulated in SI Table T1. Dynamic changes in microstructure under applied shear for the sample with 15 wt% ethanol are shown in SI Video V1.

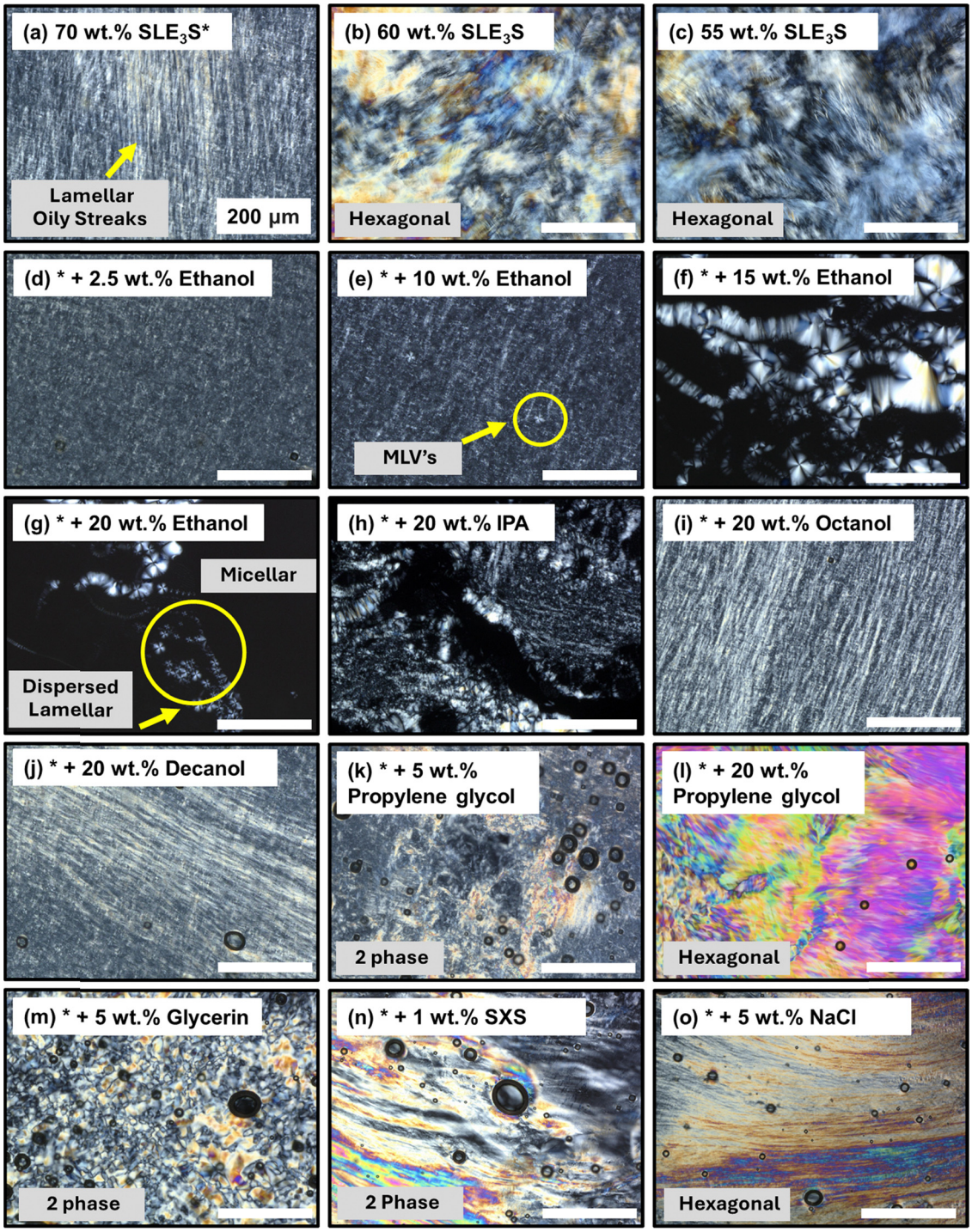

Fig. 3 (a) Neat 70 wt% lamellar SLE_3S with oily streaks and multilamellar vescicles (MLV's), (b) and (c) hexagonal 60 wt% and 55 wt% water-diluted SLE_3S control microstructures respectively. The effective surfactant concentrations for several systems with additives fall in this range. Evolution of lamellar microstructure (a) with added linear chain alcohols: (d)–(g) ethanol, (h) isopropyl alcohol (IPA), (i) octanol and (j) decanol, (k)–(o) hexagonal and mixed phases at low added propylene glycol, glycerin, sodium xylenesulfonate (SXS) and salt concentrations. Qualitative identification of phase structures is based on work by Rosevear.[10]

~17 Pa s (butanol), ~ 22 Pa s (pentanol), ~26 Pa s (hexanol), 30 Pa s (decanol) and ~35 Pa s (dodecanol) (Fig. 2(c)).

Ethanol and other short-chain, water-soluble alcohols (C_2–C_5) selectively partition into the water layers between surfactant bilayers and compete with water for interaction sites at the surfactant headgroup interface.[88–90] This disruption in local hydrogen bonding and apparent dehydration[91] of the hydration layer around SLE_3S headgroups decreases the effective headgroup area. As the hydrophobic-to-hydrophilic volume ratio increases, the CPP changes and results in a lamellar-to-micellar

transition.[13] Although ethanol strengthens hydrogen bonding in bulk water,[92] this behavior is altered in liquid crystals: in lamellar systems, ethanol displaces interfacial water and reduces water layer thickness, leading to a measurable decrease in *d*-spacing, as observed through SAXS measurements.

There is a substantial body of work studying alcohol–lipid bilayer interactions,[93,94] and the effect of short-chain linear alcohols observed here was consistent with previous findings for some other dilute surfactant systems. Friberg *et al.*[95] reported the formation of a low viscosity liquid with the addition of ethanol to the didodecyldimethylammonium bromide (DDAB)-water lamellar phase. Dynamic light scattering was used to identify the presence of aggregates in the isotropic phase. Chen *et al.*[96] and Han *et al.*[97] developed injectable low viscosity solutions by using ethanol to induce liquid–crystalline–isotropic phase transitions in the phytantriol–water system. Alam used differing wave spectroscopy (DWS) and microrheology measurements to investigate the effect of ethanol concentration and temperature on phase transitions in the Dimodan U/J monoglyceride–water system.[98] In contrast, longer-chain alcohols (C_6–C_{12}) and acetates exhibit lower solubility and preferentially partition near hydrophobic surfactant tails, acting like co-surfactants (Fig. 2(c) and (d)).[99] At the highest added dodecanol concentration (20 wt%), two lamellar phases coexisted with *d*-spacings of 46.5 ± 0.5 Å and 55.3 ± 0.8 Å. The lamellar phase with the higher *d*-spacing was more ordered (Fig. S9). The polyols, sodium xylenesulfonate and salt promoted formation of high viscosity hexagonal and mixed phases (Fig. 2(d) and 3(k)–(o)).

Approach 2: heating to approach upper temperature limit of liquid crystalline phases

Temperature-dependent viscosity reductions, azeotropic reactions[11] and other thermotropic transitions have been widely studied.[100,101] In some systems such as aqueous non-ionic pentaethylene glycol monodecyl ether ($C_{10}E_5$), modest temperatures (~35 °C) are sufficient to induce liquid crystalline-to-micellar transitions,[102] while in the linear akylbenzene sulfonate–water system studied by Stewart *et al.*, changes in headgroup-counterion interactions at elevated temperatures played a significant role.[103] Fig. 4 shows the temperature-dependent complex viscosity of 70 wt% SLE_3S paste with added polyols. While rheometry experiments were conducted within the linear viscoelastic regime, static SAXS (Fig. 5) was used to confirm that observed transitions were not shear-induced and reflected equilibrium behavior. Neat 70 wt% SLE_3S had a nearly constant complex viscosity (~108 Pa s) and lamellar structure (Fig. 5(a)) upon heating from 20 °C up to 90 °C, consistent with prior observations by Kelkar *et al.*[28] and Ferraro *et al.*[33,34] Ongoing work is exploring the interesting shift in the scattering peak (q^*) toward lower Bragg spacings with increasing temperature.

At 20 °C, the 20 wt% propylene glycol (PG) sample was hexagonal with a characteristic spacing of 49.2 ± 0.4 Å (Fig. 3(l) and 5(c)) and a complex viscosity of ~1130 Pa·s. Upon heating, the hexagonal phase persisted up to ~70 °C, beyond which higher-order SAXS peaks disappeared, and the complex viscosity dropped

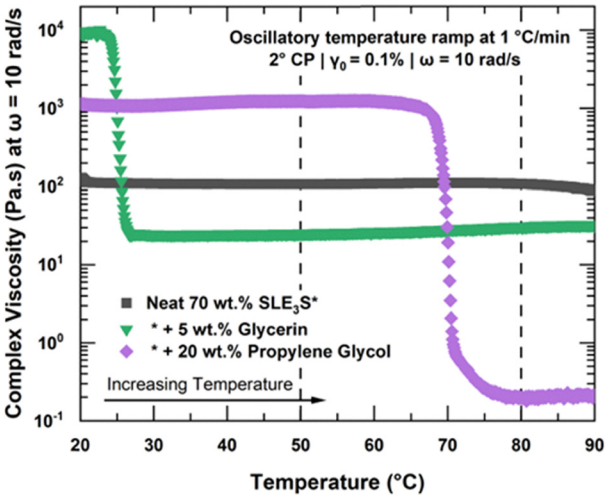

Fig. 4 Evolution of complex viscosity measured during a continuous oscillatory temperature ramp from 20 °C to 90 °C. Hexagonal to micellar phase transition for specimen with 20 wt% propylene glycol is reversible and significant hysteresis was not observed during the heating and cooling process (Fig. S10). It is key to note that temperature-driven phase transitions have both thermodynamic and kinetic aspects. Because equilibrium is governed by both heat and mass transport, the temperature ramp rate can influence observed changes.[11]

sharply to ~0.2 Pa s at 80 °C, indicating a transition to an isotropic phase with a micellar separation length of 40.6 ± 2.9 Å. In contrast, the 5 wt% glycerin sample was biphasic with at least one lamellar phase at 20 °C (*d*-spacing equal to 46.1 ± 0.5 Å and 56.7 ± 0.3 Å; Fig. 3(m) and 5(b)) with very high complex viscosity (~9248 Pa·s). While it did not transition into a micellar solution, the complex viscosity of the lamellar phase (*d*-spacing of 44 ± 0.4 Å) at 50 °C (~25 Pa s) was significantly lower than neat SLE_3S.

Polyols are water-soluble plasticizers and it is hypothesized that multiple hydroxyl groups (Fig. S1) enable strong interactions with anionic SLE_3S headgroups through hydrogen bonding.[104] These disrupt headgroup-water hydrogen bonds, potentially forming headgroup-polyol and water–polyol hydrogen bonds.[105] Thus, glycerin, with three hydroxyl groups, can form more hydrogen bonds than PG, which has two.[106] This is consistent with 1 s^{-1} viscosity measurements at 1 wt% added additive (Fig. 1(d) and Fig. S7), where the glycerin-containing sample had a higher viscosity (~31 Pa·s) than the sample with PG (~18 Pa·s). In the concentration range studied here, both glycerin and propylene glycol increase effective headgroup area, shift the CPP, and promote curvature,[107] leading to the formation of hexagonal phases. As temperature rises, thermal motion and molecular disorder increase and liquid crystals transition to an isotropic solution.[108,109] Hence, when PG-induced hexagonal phases are heated, hydrogen bonding weakens[110,111] reducing effective headgroup area. This changes the CPP again resulting in a hexagonal-to-micellar transition.

Approach 3: processing within the lamellar phase

The effects of propylene glycol (PG) and sodium chloride (NaCl) on the lamellar phase boundaries, rheology and microstructure

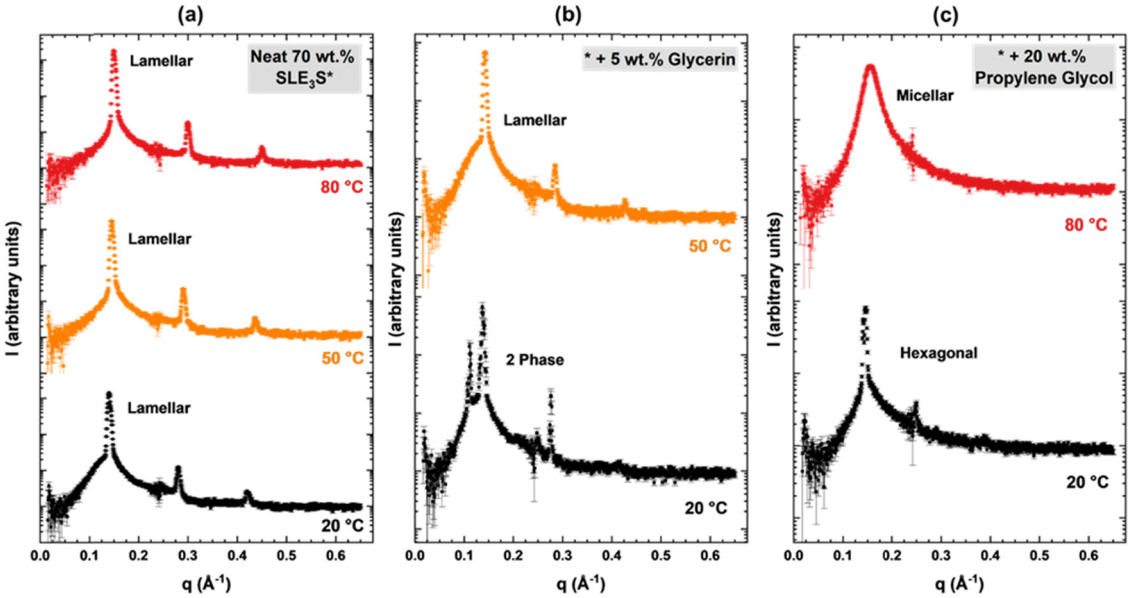

Fig. 5 Effect of heating on SAXS patterns of (a) neat 70 wt% SLE_3S, (b) +5 wt% glycerin, and (c) +20 wt% propylene glycol. Lamellar phases have characteristic peaks at q^*, $2q^*$ and $3q^*$ while hexagonal phases have peaks at q^*, $\sqrt{3}q^*$ and $2q^*$.[56] Room temperature cross-polarized micrographs are presented in Fig. 3(a), (l) and (m), and 2D scattering patterns are presented in Fig. S11.

evolution were studied in detail. Flow-phase diagrams developed by overlaying static phase information on viscosity values extracted from flow curves are presented in Fig. 6, while Fig. 7 and 8 show the evolution of lamellar microstructure with added PG and NaCl respectively. High viscosities for the neat 70 wt% SLE_1S solution at 5 °C and 10 °C are attributed to the presence of crystalline domains.[28] Behavior above room temperature is consistent with earlier observations here and in studies by Ferraro *et al.*[33,34] and Kelkar *et al.*[28] In single-phase regions at fixed additive concentration, the viscosity at 1 s^{-1}, yield stress, and flow stress (Fig. S12 and S13) all decreased with increasing temperature. The yield stress is defined as the applied stress at which irreversible plastic deformation is first observed across the sample, typically obtained by fitting a Herschel–Bulkley model and extrapolating to zero shear rate. The flow stress is the value of the shear stress at the crossover point in an amplitude sweep.[12,112] In all cases, the flow stress was numerically higher than the yield stress, potentially making it a more conservative parameter for predicting product stability and designing startup protocols in pumping to avoid stress overshoots and mechanical damage.[113] At 20 °C, 5 wt% propylene glycol had a yield stress of ~4 Pa and a flow stress of ~23 Pa while for 1 wt% NaCl, the corresponding values were ~23 Pa and ~65 Pa. Trends in two-phase regions were

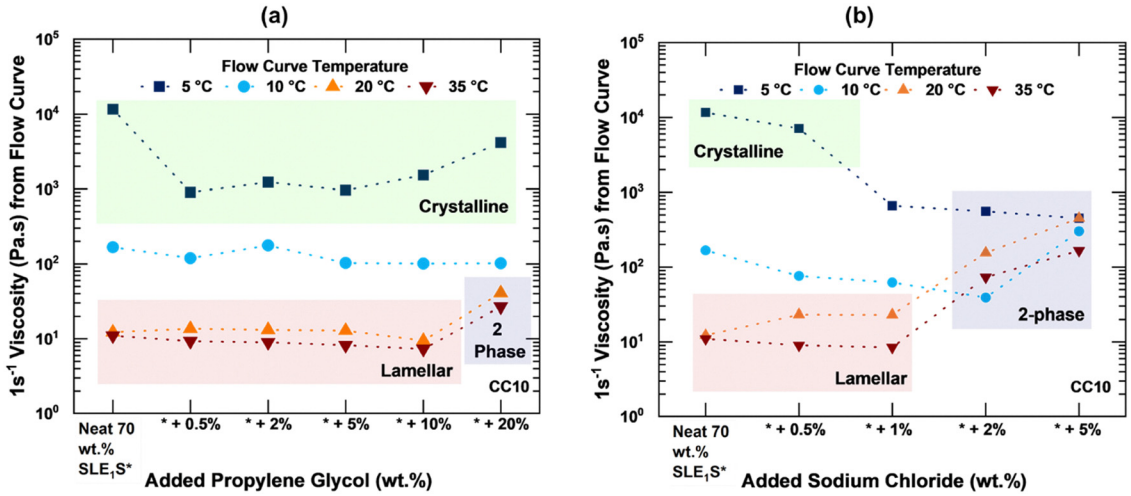

Fig. 6 Flow-phase diagrams for added (a) propylene glycol and (b) NaCl. Static phase information determined from cross-polarized optical microscopy and SAXS. Full flow curves, corresponding Herschel–Bulkley fits at low shear rates and flow stresses from amplitude sweeps are presented in Fig. S12 and S13 respectively.

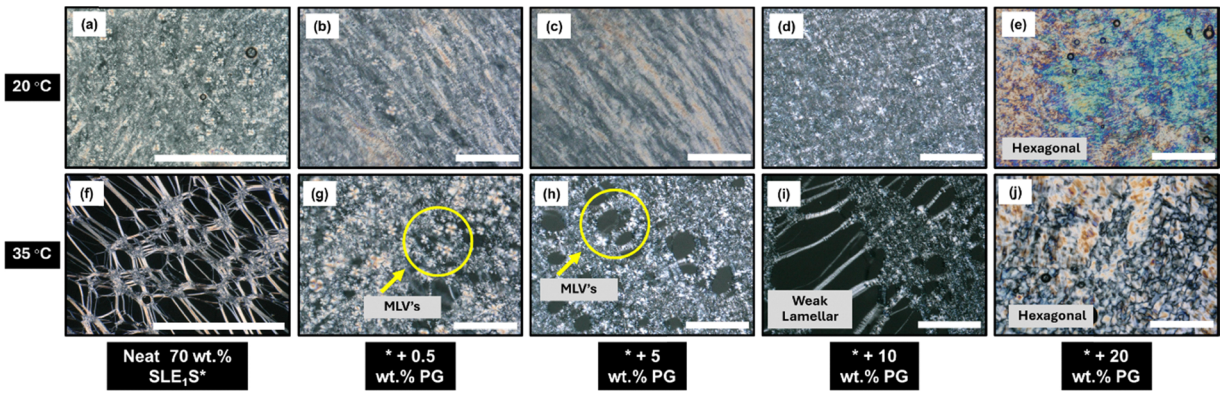

Fig. 7 Evolution of static microstructure with added propylene glycol at (b–e) 20 °C and (g–j) 35 °C. Neat Lamellar SLE_1S micrographs reproduced from Kelkar *et al.*[28] Big scale bars in (a) and (f) represent 1 mm while smaller bars represent 100 μm.

more complex, varying with relative proportions of coexisting phases.

At room temperature (~20 °C), increasing PG concentration within the lamellar region had minimal effect on 1 s^{-1} viscosity, yield stress, and flow stress up to 5 wt%, with more pronounced reductions observed only at 10 wt% PG, where the lowest 1 s^{-1} viscosity (~9.5 Pa·s) was measured. Compared to SLE_3S, the SLE_1S system exhibited a broader lamellar phase window with PG addition: while SLE_3S transitioned to a biphasic (lamellar and hexagonal) phase at PG concentrations as low as 5 wt%, SLE_1S retained a lamellar phase up to at least 10 wt%. The wider lamellar phase band in SLE_1S is likely due to its lower average degree of ethoxylation and associated PG-headgroup interactions.[33] Within the lamellar phase, for both systems, the 1 s^{-1} viscosities were comparable: SLE_1S + 2 wt% PG had viscosity of ~14 Pa s, while SLE_3S + 1 wt% PG had a viscosity of ~19 Pa s.

In contrast, salt produced a different response. Increasing the salt concentration led to a steady rise in 1 s^{-1} viscosity, yield stress, and flow stress within the lamellar phase. Across bulk SLE_nS systems the response was almost invariant with changing degree of ethoxylation. The lamellar phase boundaries between SLE_1S and SLE_3S (>2 wt%), and the 1 s^{-1} viscosities at 1 wt% NaCl (~23 Pa s for SLE_1S, ~20 Pa s for SLE_3S), were comparable. Salt affects charge screening around charged surfactant headgroups, potentially reducing headgroup repulsion and inducing phase transitions. This behavior has been studied extensively.[15,114–117]

Similar trends were observed in the static microstructure at 25 °C and 35 °C. With PG, increasing concentration and temperature progressively weakened the lamellar texture and promoted the formation of multilamellar vesicles (MLVs) (Fig. 7(g) and (h)). In contrast, while higher temperatures led to more MLVs with NaCl (Fig. 8(g)), increasing salt concentration at a fixed temperature produced fewer MLVs (Fig. 8(g) and (h)). Under applied shear, lamellar phases showed strong orientation of oily streaks, consistent with classical shear-induced alignment.[15,24,25] Aligned bilayers can roll up to form MLVs,[26] a process generally described by a balance between curvature energy and compression energy.[118] Studies investigating time-dependent evolution of microstructure and formation mechanisms of MLVs under shear, as a function of confinement, additives and temperature are ongoing.

The effect of small applied oscillations within the LVER on crystallization above the equilibrium crystallization temperature in neat lamellar phases has been previously studied by Kelkar *et al.*[28] At room temperature, the bulk lamellar phase has no crystals. As the solutions are slowly cooled, small

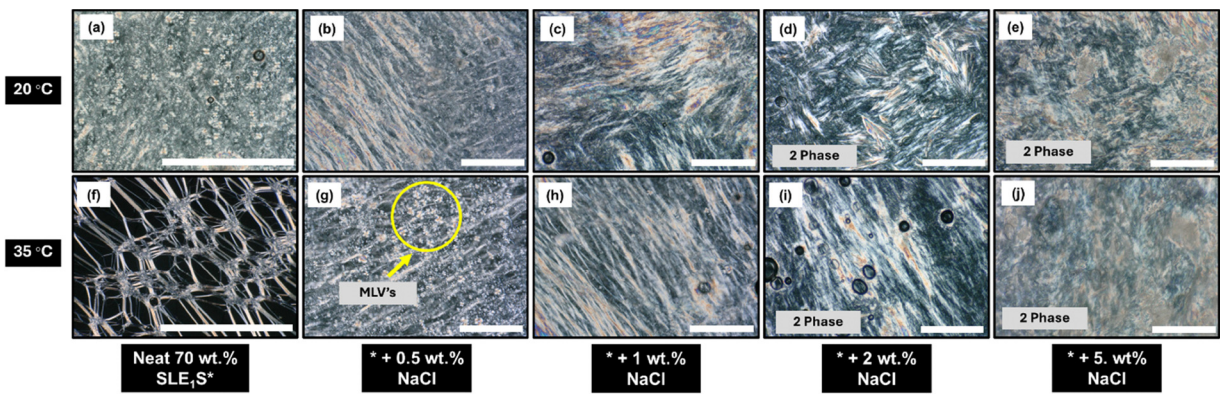

Fig. 8 Evolution of static microstructure with added common salt at (b–e) 20 °C and (g–j) 35 °C. Neat Lamellar SLE_1S micrographs reproduced from Kelkar *et al.*[28] Big scale bars in (a) and (f) represent 1 mm while smaller bars represent 100 μm.

oscillations primarily enhance growth. Inspired by the classical work of Nyvlt *et al.*[119] on the theory of metastable zones, samples with added PG and NaCl were cooled and the results are presented in Fig. 9.

Samples with added salt promoted crystallization at significantly higher temperatures than both neat 70 wt% SLE_1S and solutions with added PG. The onset temperature was also much higher than the equilibrium crystallization temperature measured by DSC and increased with increasing salt concentration. In contrast, as a known antifreeze agent,[120] PG extended the lamellar phase region and suppressed crystallization. The onset of shear-induced crystallization was restricted to temperatures close to the equilibrium DSC range. Increasing PG concentration from 2 wt% to 5 wt% had little additional effect, as both samples had nearly identical complex viscosity trends during cooling.

Macroscopic rheological measurements through flow curves provide valuable insight into bulk behavior, but internal velocity fields under shear can diverge significantly due to evolution of flow instabilities like wall slip and plug flow.[121] Wall slip refers to relative motion between the material and the boundary, resulting in a discontinuity at the wall that manifests as a sliding of the material along the surface. As the rheometer assumes a no-slip condition, wall slip leads to an apparent reduction in viscosity.[122] Plug flow describes uniform bulk translation with constant velocity across the gap where flow arises from wall slip occurring simultaneously at both confining surfaces.[123] A detailed investigation of non-homogeneous flow phenomena across different SLE_1S phases was undertaken by Caicedo-Casso *et al.*[15] their results showed that while lamellar phases typically exhibit plug flow at low and intermediate shear rates, the neat 70 wt% SLE_1S sample approached a simple shear velocity profile at 70 s^{-1}, though some slip near the rotor remained evident in the velocity profiles.

Velocity profiles for neat 70 wt% aqueous solutions of SLE_1S, SLE_2S, and SLE_3S at shear rates of 7 s^{-1} and 70 s^{-1} are presented in Fig. S14. Across all feedstock solutions, velocity profiles were qualitatively similar. At 7 s^{-1}, plug-like flow was observed, with near-uniform velocity in the gap and minor gradients near the boundaries. At 70 s^{-1}, each system exhibited simple shear near the stator and slip near the rotor, suggesting stress localization across the gap and the possible onset of shear banding. Lamellar-structured SLE_1S matched the profile reported by Caicedo-Casso *et al.*[15] only in isolated cases; more commonly, it slipped more near the rotor. These differences were not unexpected and are likely due to batch-to-batch variability.

The effects of PG addition are presented in Fig. 10. At 7 s^{-1}, all samples showed plug-flow with nearly constant velocity across the gap (Fig. 10(c)). The 10 wt% PG sample slips more at both walls with the lowest velocity across the gap. It also shows the lowest measured shear stress on the flow curve −28 Pa compared to 33 Pa for neat SLE_1S. The flow behavior was different at 70 s^{-1} – all specimens showed simple shear behavior closest to the stator and wall slip at the rotor. The 5 wt% PG sample was like the neat SLE_1S, but the 10 wt% PG solution slipped more (Fig. 10(d)) and had the lowest measured shear stress (~107 Pa *vs.* ~116 Pa for neat SLE_1S; Fig. 10(b)). However, the normalized velocity near the rotor was slightly higher than that observed at 7 s^{-1}. This is likely due to wall slip being more dominant at lower shear rates.[112,124]

The increase in slip with 10 wt% PG addition, suggests that PG alters bilayer-shearing surface interactions. As a plasticizer, it weakens the lamellar structure (Fig. 7(c), (e) and (g)) and the less structured lamellar bilayers may align more readily under shear, acting as localized lubrication layers. Since increased surface roughness reduces wall slip,[125] formation of aligned PG-rich bilayers should have the opposite effect and facilitate

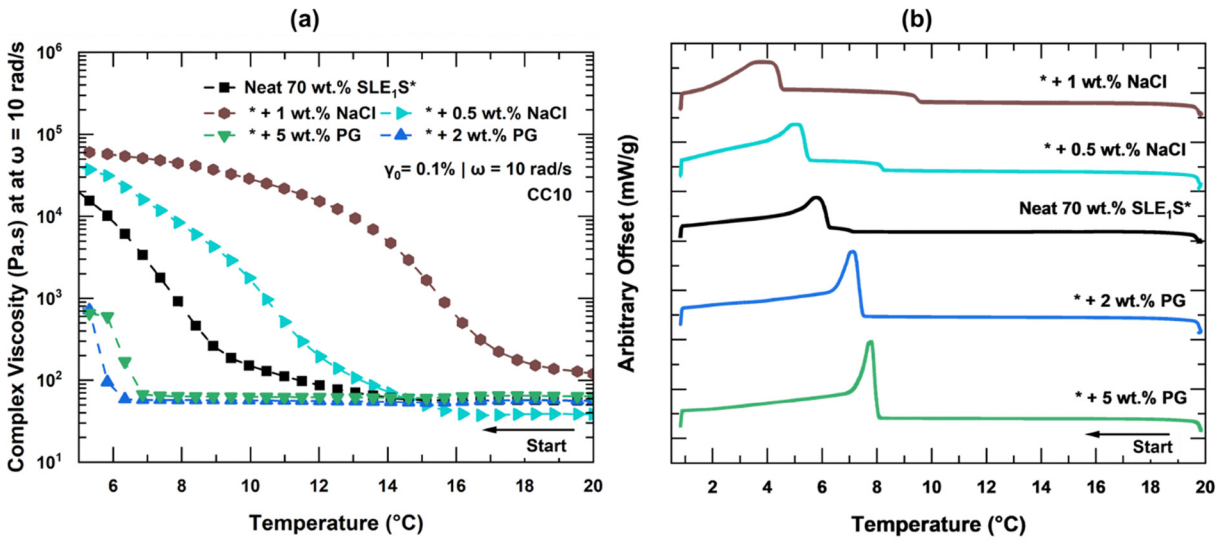

Fig. 9 (a) Effect of small applied oscillations on the complex viscosity, and (b) equilibrium crystallization temperature range in a DSC ramp. Specimens were cooled from 20 °C to 5 °C at 1 °C min^{-1}. Onset of crystallization is inferred from the drastic increase in complex viscosity during cooling.

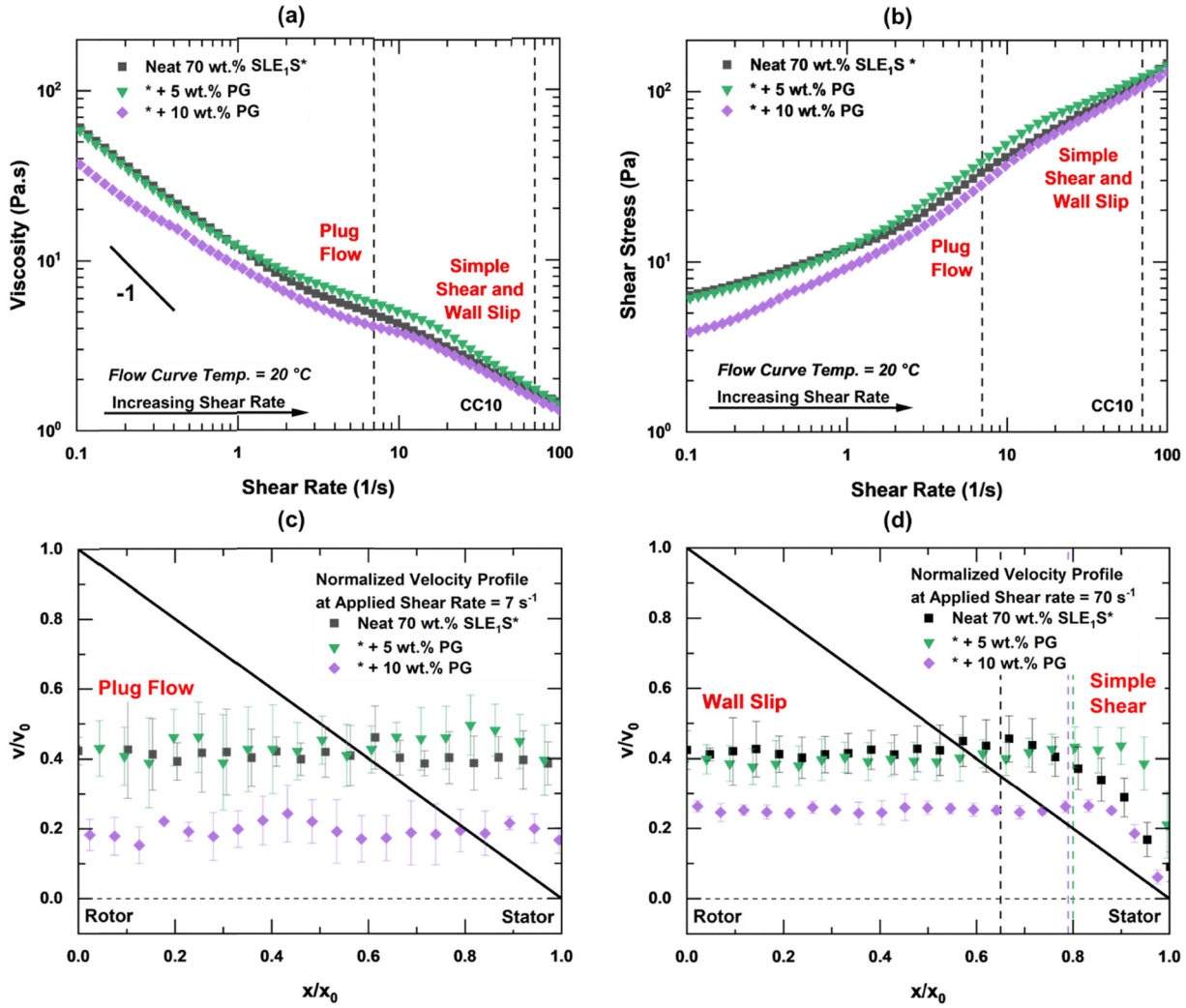

Fig. 10 Effect of propylene glycol (PG) addition on bulk rheology and velocity profiles of 70 wt% SLE_1S solutions. (a) and (b) viscosity and shear stress as a function of shear rate at 20 °C. Vertical dashed lines indicate shear rates corresponding to USV measurements, (c) and (d) normalized velocity profiles at 7 s^{-1} and 70 s^{-1}. Solid black line indicates slope of −1.

slip. These observations are consistent with a slip-film mechanism,[126] where a structurally relaxed or weaker layer near the rotor wall accommodates shear independently of the bulk. Due to instrumental resolution limitations, the thickness of such a layer is not directly measured here, but the combination of increased slip and weakened structure supports this interpretation. For more detailed discussions of flow instabilities in complex fluids, the reader is directed to the works of Divoux *et al.*,[124] Cloitre and Bonnecaze,[127] and Malkin and Patlazhan.[128]

Implications

Processing highly viscous, concentrated feedstocks is a key challenge in surfactant manufacturing. Upstream operations routinely face a cost-driven trade-off between increased energy demands for processing and the added complexity of introducing additives. The primary goal of utilizing additives is to maintain high activity while reducing viscosity, and the strategies demonstrated here (summarized in Fig. 11) with lamellar phases suggest that this constraint may not be absolute.

Short-chain alcohols effectively reduced viscosity, but flammability and volatility concerns may limit their use in early-stage processing – particularly in heated premix vessels or open transfer systems. When introduced too early, alcohols can limit the use of temperature as a downstream processing lever, requiring all subsequent additives to be miscible at lower temperatures and not induce liquid–crystalline order. While counterintuitive, passing through a hexagonal phase before heating, despite its higher viscosity, can lead to lower viscosity manufacturing pathways. In typical manufacturing processes, a formula may be structured into a hexagonal phase and held hot in a jacketed main mix tank to induce a transition to a micellar solution. After this, performance ingredients like conditioning polymers or mildness boosters can be introduced while the system is still hot followed by alcohols during cooling to tune

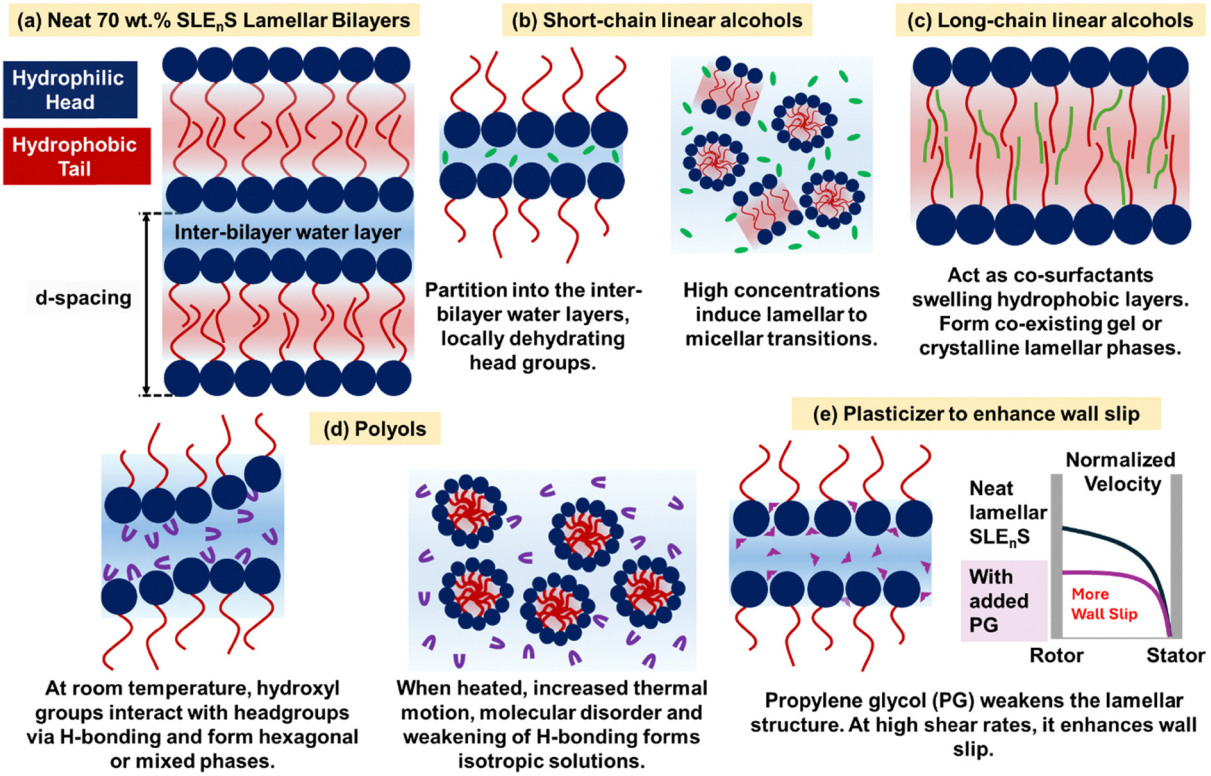

Fig. 11 Schematic of three approaches to simplify processing of concentrated feedstock pastes. (a) Structure of the lamellar feedstock, (b) and (c) approach 1: linear chain alcohols, (d) approach 2: heating to approach upper temperature limit of liquid crystalline phases, and (e) approach 3: processing within the lamellar phase by enhancing wall slip. Adapted and modified from Seddon and Templer,[129] Kulkarni,[130] Radaic *et al.*,[131] and Steck *et al.*[132]

rheology. A similar order-of-addition dependence has been reported for feedstock alkyl ether sulfate systems, where ionic liquid–alcohol blends reduced viscosity only when introduced together at low concentrations; when added separately, they had little to no effect.[133]

Hexagonal phases formed inside pipe loops – often triggered by trace water and thought to be irreversible, can catastrophically obstruct handling and compromise throughput. In some cases, entire sections must be replaced, resulting in costly downtime. But, if they are intentionally formed with the right additives in tanks or vessels that can be heated and mixed, they are more manageable and even useful. At room temperature, their high viscosity and yield stress can help prevent spills or dripping. In solutions that remain lamellar throughout processing, flow can be tuned without inducing bulk phase transitions. Additives that induce wall slip and suppress shear-induced crystallization can improve flow rates[134,135] and reduce the formation of high-viscosity crystalline phases in pipes and pumps under minor temperature variations.

Beyond lamellar SLE$_n$S systems, formulators should first identify the liquid crystalline phase formed by their concentrated feedstock without additives using a simple dilution series and cross-polarized optical microscopy. The combination of approaches needed to reach a low-viscosity micellar solution will depend on this initial phase, since efficient trajectories through complex phase diagrams necessitate a clearly defined starting point. Instead of relying on simplistic CPP or hydrophilic–lipophilic balance (HLB), the hydrophilic–lipophilic deviation (HLD)-net average curvature (NAC) framework offers a quantitative basis for anticipating how additives can modify spontaneous curvature.[136,137] In systems containing oils, fragrances, or co-solvents, shifts in effective alkane carbon number (EACN) become equally important.[137] The additive effects demonstrated here can be reinterpreted through this lens. When designed to selectively target the headgroup, tail, or water layers, additive blends can tune rheology, suppress shear-induced crystallization and function as value-added formulation ingredients.

Conclusions

In this experimental study, three additive-driven approaches to tune the rheology and microstructure of concentrated lamellar structured 70 wt% SLE$_n$S–water systems are demonstrated (Fig. 11). Short-chain alcohols such as ethanol and isopropyl alcohol reduced viscosity by locally dehydrating headgroups and inducing lamellar-to-micellar transitions at high concentrations (Fig. 2 and 3(d)–(h)). Glycerin and propylene glycol interact with SLE$_n$S headgroups *via* hydrogen bonding, inducing lamellar-to-hexagonal or mixed-phase transitions at room temperature, and form micellar liquids upon heating beyond the upper temperature limit of liquid crystalline phases (Fig. 4 and 5).

Within the lamellar phase, PG weakened bilayer structure (Fig. 7), suppressed shear-induced crystallization (Fig. 9) and

enhanced wall slip at high shear rates (Fig. 10). Its effects also depended more strongly on the degree of ethoxylation than those of salt. By contrast, NaCl led to higher-viscosity biphasic regions at low concentrations (Fig. 6 and 8) and promoted shear-induced crystallization above the equilibrium crystallization temperature (Fig. 9). Datasets developed here – linking additive structure to rheology, *d*-spacing, and yield stress – can further support modeling efforts aimed at designing tailor-made molecules to achieve targeted flow and structural outcomes. Workflows developed here for SLE$_n$S systems provide a foundation for optimizing processing and enabling the sustainable design and manufacturing of concentrated surfactant-based products.

Author contributions

P. U. K.: conceptualization, data curation, formal analysis, investigation, methodology, visualization, writing – original draft; M. K.: data curation, formal analysis, investigation, methodology, visualization, writing – review & editing; C. A. A.: investigation, writing – review & editing; E. R. W.: investigation, writing – review & editing; S. L.: conceptualization, funding acquisition, resources, writing – review & editing; K. A. E.: conceptualization, data curation, funding acquisition, project administration, visualization, supervision, writing – original draft, writing – review & editing.

Conflicts of interest

There are no conflicts of interest to declare.

Data availability

Data supporting this article have been included as part of the SI.

Molecular structures of all molecules, characterization of various SLE$_n$S feedstocks, calibration curves for the rheo-USV, SAXS patterns for key phases and transitions, full flow curves and shear stress vs shear rate data at low shear rates with tabulated Herschel–Bulkley fits for all additives, amplitude sweeps and flow stress at different temperatures, rheo-USV velocity profiles of neat SLE$_n$S feedstocks. See Doi: **https://doi.org/10.1039/d5sm00597c**

Acknowledgements

P. U. K. and K. A. E. acknowledge support from the National Science Foundation (NSF) through GOALI grant no. CBET-2112956.

References

1 J. Scamehorn, D. Sabatini and J. Harwell, *Encyclopedia of Supramolecular Chemistry*, CRC Press, Boca Raton, 1st edn, 2004.
2 J. Scamehorn, D. Sabatini and J. Harwell, *Encyclopedia of Supramolecular Chemistry*, CRC Press, Boca Raton, 1st edn, 2004.
3 S. Liu, L. G. Papageorgiou and N. Shah, *Comput. Ind. Eng.*, 2020, **139**, 106189.
4 J. Cosby, PhD thesis, University of Sheffield, 2021.
5 E. Saouter, G. van Hoof, C. A. Pittinger and T. C. J. Feijtel, *Int. J. Life Cycle Assess.*, 2001, **6**, 363–372.
6 M. Giagnorio, A. Amelio, H. Grüttner and A. Tiraferri, *J. Cleaner Prod.*, 2017, **154**, 593–601.
7 F. Mattos Batista de Moraes, L. Kulay and A. Trianni, *Sustainable Prod. Consum.*, 2025, **55**, 76–89.
8 I. E. M. O. de Moura and E. A. da Silva, *Int. J. Environ. Sci. Technol.*, 2024, **21**, 3235–3256.
9 R. Zana, *Dynamics of Surfactant Self-Assemblies*, CRC Press, 1st edn, 2005.
10 F. B. Rosevear, *J. Am. Oil Chem. Soc.*, 1954, **31**, 628–639.
11 R. G. Laughlin, *The Aqueous Phase Behavior of Surfactants*, Academic Press, 1994.
12 R. G. Larson, *The Structure and Rheology of Complex Fluids*, Oxford Academic Press, 1998.
13 J. N. Israelachvili, D. J. Mitchell and B. W. Ninham, *J. Chem. Soc., Faraday Trans. 2*, 1976, **72**, 1525.
14 P. A. Hassan, G. Verma and R. Ganguly, *Functional Materials*, Elsevier, 2012, pp. 1–59.
15 E. A. Caicedo-Casso, J. E. Bice, L. R. Nielsen, J. L. Sargent, S. Lindberg and K. A. Erk, *Rheol. Acta*, 2019, **58**, 467–482.
16 E. F. Marques and B. F. B. Silva, *Encyclopedia of Colloid and Interface Science*, Springer Berlin Heidelberg, Berlin, Heidelberg, 2013, pp. 1290–1333.
17 M. Aljabri and T. Rodgers, *ACS Phys. Chem. Au*, 2024, **4**, 490–498.
18 P. Kelkar, M. Caggioni, K. A. Erk and S. Lindberg, *Langmuir*, 2025, **41**, 4334–4344.
19 A. Capaccio, S. Caserta, S. Guido, G. Rusciano and A. Sasso, *J. Colloid Interface Sci.*, 2020, **561**, 136–146.
20 R. H. Ewoldt, M. T. Johnston and L. M. Caretta, *Experimental Challenges of Shear Rheology: How to Avoid Bad Data, Complex Fluids in Biological Systems. Biological and Medical Physics, Biomedical Engineering*. Springer, New York, NY, 2015, pp. 207–241.
21 D. Coles, *J. Fluid Mech.*, 1965, **21**, 385–425.
22 C. D. Andereck, S. S. Liu and H. L. Swinney, *J. Fluid Mech.*, 1986, **164**, 155–183.
23 M. Wlodzimierz Sulek and A. Bak, *Int. J. Mol. Sci.*, 2010, **11**, 189–205.
24 P. Sierro and D. Roux, *Phys. Rev. Lett.*, 1997, **78**, 1496–1499.
25 O. Diat, D. Roux and F. Nallet, *J. Phys. II*, 1993, **3**, 1427–1452.
26 D. Roux, F. Nallet and O. Diat, *Europhys. Lett.*, 1993, **24**, 53–58.
27 M. G. Berni, C. J. Lawrence and D. Machin, *Adv. Colloid Interface Sci.*, 2002, **98**, 217–243.
28 P. U. Kelkar, M. Kaboolian, R. D. Corder, M. Caggioni, S. Lindberg and K. A. Erk, *Soft Matter*, 2024, **20**, 3299–3312.
29 P. Kékicheff, C. Grabielle-Madelmont and M. Ollivon, *J. Colloid Interface Sci.*, 1989, **131**, 112–132.
30 R. I. Castaldo, R. Pasquino, M. M. Villone, S. Caserta, C. Gu, N. Grizzuti, S. Guido, P. L. Maffettone and V. Guida, *Soft Matter*, 2019, **15**, 8352–8360.

31 R. L. Hendrikse, A. E. Bayly and P. K. Jimack, *J. Phys. Chem. B*, 2022, **126**, 8058–8071.
32 R. L. Hendrikse, A. E. Bayly, P. K. Jimack and X. Lai, *J. Phys. Chem. B*, 2023, **127**, 4676–4686.
33 R. Ferraro, M. Michela Salvatore, R. Esposito, S. Murgia, S. Caserta, G. D'Errico and S. Guido, *J. Mol. Liq.*, 2024, **405**, 124990.
34 R. Ferraro and S. Caserta, *Rheol. Acta*, 2023, **62**, 365–375.
35 S. Abbott, Pure versus Commercial Surfactants, **https://www.stevenabbott.co.uk/practical-surfactants/Pure-Commercial.php**, (accessed 19 May 2025).
36 P. Romanowski and R. Schueller, *Beginning cosmetic chemistry: practical knowledge for the cosmetic industry*, Allured Books, Carol Stream, 3rd edn, 2009.
37 M. Chandler and S. Gahan, Introducing the '4-P+ Process' to Power Production of Natural Products, **https://www.in-cosmetics.com/global/en-gb/show-programme/sessions-details.4266.236496.Introducing%2Bthe%2B%25E2%2580%25984-P%252B%2BProcess%25E2%2580%2599%2Bto%2BPower%2BProduction%2Bof%2BNatural%2BProducts.html**, (accessed 19 May 2025).
38 S. Abbott, *Surfactant Science: Principles & Practice, 1.0.7.*, 2024, pp. 198–213.
39 J. W. McBain and W. J. Elford, *J. Chem. Soc.*, 1926, **129**, 421–438.
40 P. Ekwall, *Advances in Liquid Crystals*, 1975, vol. 1, pp. 1–142.
41 P. Ekwall, L. Mandell and K. Fontell, *J. Colloid Interface Sci.*, 1969, **29**, 639–646.
42 R. De Lisi and S. Milioto, *Chem. Soc. Rev.*, 1994, **23**, 67–73.
43 R. G. Laughlin, *J. Am. Oil Chem. Soc.*, 1990, **67**, 705–710.
44 A. Khan, *Curr. Opin. Colloid Interface Sci.*, 1996, **1**, 614–623.
45 K. Holmberg, B. Jönsson, B. Kronberg and B. Lindman, *Surfactants and Polymers in Aqueous Solution*, Wiley, 2002, pp. 67–96.
46 H. Wennerström, *J. Dispers. Sci. Technol.*, 2007, **28**, 31–37.
47 I. M. Tucker, *Curr. Opin. Colloid Interface Sci.*, 2024, **71**, 101789.
48 G. Rong and S. E. Friberg, *J. Dispers. Sci. Technol.*, 1988, **9**, 401–413.
49 S. E. Friberg and P. Liang, *Colloid Polym. Sci.*, 1986, **264**, 449–453.
50 M. Buzier and J.-C. Ravey, *Surfactants in Solution*, Springer US, Boston, MA, 1986, pp. 525–536.
51 R. Strey, *Bunsen-Ges. Phys. Chem., Ber.*, 1996, **100**, 182–189.
52 D. Roux, C. R. Safinya and F. Nallet, *Micelles, Membranes, Microemulsions, and Monolayers*, 1994, pp. 303–346.
53 A. S. Sadaghiani, A. Khan and B. Lindman, *J. Colloid Interface Sci.*, 1989, **132**, 352–362.
54 Y. Tokuoka, H. Uchiyama and M. Abe, *Colloid Polym. Sci.*, 1994, **272**, 317–323.
55 C. Ligoure, G. Bouglet and G. Porte, *Phys. Rev. Lett.*, 1993, **71**, 3600–3603.
56 P. Alexandridis, U. Olsson and B. Lindman, *Langmuir*, 1998, **14**, 2627–2638.
57 G. Karlstroem, A. Carlsson and B. Lindman, *J. Phys. Chem.*, 1990, **94**, 5005–5015.
58 M. Kahlweit, R. Strey, P. Firman and D. Haase, *Langmuir*, 1985, **1**, 281–288.
59 T. Wärnheim and A. Jönsson, *J. Colloid Interface Sci.*, 1988, **125**, 627–633.
60 T. Wärnheim, A. Jönsson and M. Sjöberg, *Surfactants and Macromolecules: Self-Assembly at Interfaces and in Bulk*, Steinkopff, Darmstadt, 1990, pp. 271–279.
61 K. P. Das, A. Ceglie, M. Monduzi, O. Söderman and B. Lindman, *New Trends in Colloid Science*, Steinkopff, Darmstadt, 1987, pp. 167–173.
62 N. Akter, S. Radiman, F. Mohamed, I. A. Rahman and M. I. H. Reza, *Sci. Rep.*, 2011, **1**, 71.
63 A. Baruah, A. K. Pathak and K. Ojha, *Ind. Eng. Chem. Res.*, 2015, **54**, 7640–7649.
64 Z. Zhong, G. Du, Y. Wang and J. Jiang, *Langmuir*, 2023, **39**, 11081–11089.
65 H. Honaryar, S. Amirfattahi, D. Nguyen, K. Kim, J. C. Shillcock and Z. Niroobakhsh, *Small*, 2024, **20**(42), DOI: **10.1002/smll.202403013**.
66 K. A. Murthy and E. W. Kaler, *Colloid Polym. Sci.*, 1989, **267**, 330–335.
67 G. Montalvo, M. Valiente and E. Rodenas, *Langmuir*, 1996, **12**, 5202–5208.
68 A. Martino and E. W. Kaler, *Colloids Surf., A*, 1995, **99**, 91–99.
69 J. Yang, X. Wang, S. Ji, X. Wang, W. Qin and R. Li, *J. Mol. Liq.*, 2016, **213**, 8–12.
70 R. A. Gonçalves, B. Lindman, M. G. Miguel, T. Iwata and Y. M. Lam, *J. Colloid Interface Sci.*, 2018, **528**, 400–409.
71 R. A. Gonçalves, P. Naidjonoka, T. Nylander, M. G. Miguel, B. Lindman and Y. M. Lam, *RSC Adv.*, 2020, **10**, 18025–18034.
72 R. A. Gonçalves, Y.-M. Lam and B. Lindman, *Molecules*, 2021, **26**, 3946.
73 L. Piculell, *Langmuir*, 2013, **29**, 10313–10329.
74 A. Cukurkent and O. Masalci, *Colloid Polym. Sci.*, 2025, **303**, 301–312.
75 S. Khosharay, M. Rahmanzadeh and B. ZareNezhad, *Int. J. Thermophys.*, 2020, **41**, 166.
76 F. Choi, R. Chen and E. J. Acosta, *J. Colloid Interface Sci.*, 2020, **564**, 216–229.
77 M. Pleines, W. Kunz, T. Zemb, D. Benczédi and W. Fieber, *J. Colloid Interface Sci.*, 2019, **537**, 682–693.
78 A. Parker and W. Fieber, *Soft Matter*, 2013, **9**, 1203–1213.
79 M. Panoukidou, C. R. Wand, A. Del Regno, R. L. Anderson and P. Carbone, *J. Colloid Interface Sci.*, 2019, **557**, 34–44.
80 M. T. Hossain and R. H. Ewoldt, *J. Rheol.*, 2024, **68**, 113–144.
81 J. E. Bice, *Master of Science in Materials Science Engineering*, Purdue University, 2017.
82 S. Manneville, L. Bécu and A. Colin, *Eur. Phys. J.: Appl. Phys.*, 2004, **28**, 361–373.
83 J. S. Clunie, J. F. Goodman and P. C. Symons, *Trans. Faraday Soc.*, 1969, **65**, 287.

84 J. W. Gibbs, *The Collected Works of J. Willard Gibbs*, Longmans, Green and Co., New York, 1928, vol. I.
85 G. Kaptay, *Materials*, 2024, **17**, 6048.
86 Y. Yamashita, H. Kunieda, E. Oshimura and K. Sakamoto, *J. Colloid Interface Sci.*, 2007, **312**, 172–178.
87 Y. Yamashita, *Liquid Crystals – Recent Advancements in Fundamental and Device Technologies*, InTech, 2018.
88 W. R. Klemm, *Alcohol*, 1990, **7**, 49–59.
89 S. Cinelli, G. Onori and A. Santucci, *Colloids Surf., A*, 1999, **160**, 3–8.
90 L. Toppozini, C. L. Armstrong, M. A. Barrett, S. Zheng, L. Luo, H. Nanda, V. G. Sakai and M. C. Rheinstädter, *Soft Matter*, 2012, **8**, 11839.
91 J.-S. Chiou, P. R. Krishna, H. Kamaya and I. Ueda, *Biochim. Biophys. Acta, Biomembr.*, 1992, **1110**, 225–233.
92 F. Li, Z. Men, S. Li, S. Wang, Z. Li and C. Sun, *Spectrochim. Acta, Part A*, 2018, **189**, 621–624.
93 M. Patra, E. Salonen, E. Terama, I. Vattulainen, R. Faller, B. W. Lee, J. Holopainen and M. Karttunen, *Biophys. J.*, 2006, **90**, 1121–1135.
94 H. A. Pillman and G. J. Blanchard, *J. Phys. Chem. B*, 2010, **114**, 3840–3846.
95 S. E. Friberg, H. Hasinović, Q. Yin, Z. Zhang and R. Patel, *Colloids Surf., A*, 1999, **156**, 145–156.
96 Y. Chen, X. Liang, P. Ma, Y. Tao, X. Wu, X. Wu, X. Chu and S. Gui, *AAPS PharmSciTech*, 2015, **16**, 846–854.
97 K. Han, X. Pan, M. Chen, R. Wang, Y. Xu, M. Feng, G. Li, M. Huang and C. Wu, *Eur. J. Pharm. Sci.*, 2010, **41**, 692–699.
98 M. M. Alam, *Liq. Cryst.*, 2012, **39**, 1427–1434.
99 S. Abbott, *Surfactant Science: Principles and Practice*, 2019, vol. 1.0.6.
100 H. Kunieda and F. Harigai, *J. Colloid Interface Sci.*, 1990, **134**, 585–588.
101 H. Kunieda and K. Nakamura, *J. Phys. Chem.*, 1991, **95**, 1425–1430.
102 Y. Nibu and T. Inoue, *J. Colloid Interface Sci.*, 1998, **205**, 305–315.
103 J. A. Stewart, A. Saiani, A. Bayly and G. J. T. Tiddy, *Colloids Surf., A*, 2009, **338**, 155–161.
104 Q. Li, X. Wang, X. Yue and X. Chen, *Langmuir*, 2015, **31**, 13511–13518.
105 N. H. Rhys, R. J. Gillams, L. E. Collins, S. K. Callear, M. J. Lawrence and S. E. McLain, *J. Chem. Phys.*, 2016, **145**, DOI: 10.1063/1.4971208.
106 X. Pei, Y. You, J. Zhao, Y. Deng, E. Li and Z. Li, *J. Colloid Interface Sci.*, 2010, **351**, 457–465.
107 K. Alfons and S. Engstrom, *J. Pharm. Sci.*, 1998, **87**, 1527–1530.
108 A. de Vries, *Liquid Crystals and Ordered Fluids*, Springer US, Boston, MA, 1984, pp. 137–153.
109 K. Aramaki, U. Olsson, Y. Yamaguchi and H. Kunieda, *Langmuir*, 1999, **15**, 6226–6232.
110 C. Czeslik and J. Jonas, *Chem. Phys. Lett.*, 1999, **302**, 633–638.
111 M. Hu, J. Zhou, L. Jiang, Z. Wang, Y. Bao and S. Cui, *J. Phys. Chem. B*, 2025, **129**, 4547–4557.
112 C. W. Macosko, *Rheology: Principles, Measurements, and Applications*, Wiley-VCH, New York, 1994.
113 S. K. Romberg and A. P. Kotula, *Addit. Manuf.*, 2023, **71**, 103589.
114 Y. Aota-Nakano, S. J. Li and M. Yamazaki, *Biochim. Biophys. Acta, Biomembr.*, 1999, **1461**, 96–102.
115 S. J. Li, Y. Yamashita and M. Yamazaki, *Biophys. J.*, 2001, **81**, 983–993.
116 B. W. Muir, G. Zhen, P. Gunatillake and P. G. Hartley, *J. Phys. Chem. B*, 2012, **116**, 3551–3556.
117 A. S. Rafique, S. Khodaparast, A. S. Poulos, W. N. Sharratt, E. S. J. Robles and J. T. Cabral, *Soft Matter*, 2020, **16**, 7835–7844.
118 L. Donina, A. Rafique, S. Khodaparast, L. Porcar and J. T. Cabral, *Soft Matter*, 2021, **17**, 10053–10062.
119 J. Nyvlt, O. Sohnel, M. Matuchova and M. Broul, *The Kinetics of industrial crystallization*, Elsevier, Amsterdam, 1985.
120 B. C. Bhattarai, A. Parajuli and K. B. Stiansen-Snoerud, *Front. Environ. Eng.*, 2025, **3**, DOI: 10.3389/fenve.2024.1519115.
121 C. Poelma, *Exp. Fluids*, 2017, **58**, 3.
122 A. Talmon, E. Meshkati and F. van Rees, *The 20th International Conference on Transport and Sedimentation of Solid Particles. 50th anniversary*, Wydawnictwo Uniwersytetu Przyrodniczego we Wrocławiu (WUELS Publishing House)), 2023, pp. 171–182.
123 S. Lerouge and J.-F. Berret, *Advances in Polymer Science*, 2009, pp. 1–71.
124 T. Divoux, M. A. Fardin, S. Manneville and S. Lerouge, *Annu. Rev. Fluid Mech.*, 2016, **48**, 81–103.
125 A. Abbasi Moud, J. Piette, M. Danesh, G. C. Georgiou and S. G. Hatzikiriakos, *J. Rheol.*, 2022, **66**, 79–90.
126 D. Kleinschmidt and V. Schöppner, *SPE Polym.*, 2023, **4**, 63–79.
127 M. Cloitre and R. T. Bonnecaze, *Rheol. Acta*, 2017, **56**, 283–305.
128 A. Y. Malkin and S. A. Patlazhan, *Adv. Colloid Interface Sci.*, 2018, **257**, 42–57.
129 J. M. Seddon and R. H. Templer, in *Handbook of Biological Physics – Structure and Dynamics of Membranes: From Cells to Vesicles*, ed. R. Lipowsky and R. Sackmann, 1995, vol. 1, pp. 97–160.
130 C. V. Kulkarni, *Nanoscale*, 2012, **4**, 5779.
131 A. Radaic, L. R. S. Barbosa, C. Jaime, Y. L. Kapila, F. B. T. Pessine and M. B. de Jesus, *Advances in Biomembranes and Lipid Self-Assembly*, 2016, vol. 24, pp. 1–42.
132 K. Steck, C. Schmidt and C. Stubenrauch, *Gels*, 2018, **4**, 78.
133 D. T. Piorkowski and D. S. Stott, Use of an Ionic Liquid and Alcohol Blend to Modify the Rheology of Polyethoxylated Alcohol Sulfates, US11028342B2, 2017.
134 X. Ma, Y. Duan and H. Li, *Powder Technol.*, 2012, **230**, 127–133.
135 L. Chen, Y. Duan, C. Zhao and L. Yang, *Chem. Eng. Process.*, 2009, **48**, 1241–1248.
136 E. J. Acosta, *Colloids Surf., A*, 2008, **320**, 193–204.
137 E. Acosta, J. Harwell and D. A. Sabatini, *Surfactant Formulation Engineering using HLD and NAC*, Academic Press and AOCS Press, 1st edn, 2025.

